Detection of Renal Hypoxia Configuration in Patients with Lupus Nephritis: A Primary Study Using Blood Oxygen Level–Dependent MR Imaging

Zhengfeng Zheng
Tianjin Medical University General Hospital
Yanyan Wang
Tianjin Medical University General Hospital
Tiekun Yan
Tianjin Medical University General Hospital
Junya Jia
Tianjin Medical University General Hospital
Dong Li
Tianjin Medical University General Hospital
Li Wei
Tianjin Medical University General Hospital
Wenya Shang
Tianjin Medical University General Hospital
huilan shi (shihuilan@vip.126.com)
Tianjin Medical University General Hospital

Research article

Keywords: Lupus nephritis; Blood oxygen level dependent; Renal hypoxia; Magnetic resonance imaging

Posted Date: March 3rd, 2020

DOI: https://doi.org/10.21203/rs.2.11872/v3

Version of Record: A version of this preprint was published at Abdominal Radiology on October 20th, 2020. See the published version at https://doi.org/10.1007/s00261-020-02794-y.

Abstract

Background Renal microstructure and function are closely associated with homeostasis of oxygenation. Analyzing renal blood oxygen level–dependent (BOLD) magnetic resonance imaging (MRI) examination results will provide information on the biological status of the kidneys. The current study was performed to explore the hypoxia mode of the entire renal parenchyma in patients with lupus nephritis (LN). Methods Twenty-three adult patients with LN and eighteen healthy volunteers were recruited. R2* values were acquired through the use of the BOLD MRI analysis technique. The narrow rectangular region of interest was used to explore the hypoxia configuration in entire depths of renal parenchyma. Acquired sequential R2* data were fitted by using four categories of mathematic functions. The tendency of R2* data in both patients with LN and healthy volunteers was also compared through the use of repeated-measures analysis of variance. Results R2* data from the superficial cortex to deep medulla displayed two patterns, called a sharp uptrend style and a flat uptrend style. After sequential R2* data were fitted individually with the use of four mathematic formulas, the multiple-compartment Gaussian function showed the highest goodness of fit. Compared with two categories of R2* value styles, the R2* tendency of entire parenchyma in patients with LN was different from that in healthy volunteers. Conclusions Deep renal medullary oxygenation was not always overtly lower than oxygenation in superficial renal cortical zone. Renal parenchyma oxygenation manifestation could be described through the use of a Gaussian function model. The deoxygenation tolerance capability was damaged in patients with LN.

Background

Lupus nephritis (LN) is the primary cause of secondary glomerulonephritis in patients in China [1]. Renal microstructure and function changes are closely associated with glomerular function and kidney prognosis. Precise evaluation of renal pathophysiological injuries is key in the treatment of patients with LN [2, 3]. Unfortunately, there are no ideal methods of simultaneously detecting renal structure and pathophysiological status. Although renal biopsy specimen examination has been successfully applied in clinical practice for several decades, this technique is not considered to be ideal because of multiple inherent shortcomings, such as serious bleeding complications [4], incommodious field of view for inspection, and limited biopsy specimen locations. Therefore, a new, noninvasive, comprehensive assessment method is needed.

By using the paramagnetic properties of deoxyhemoglobin, the blood oxygen level–dependent (BOLD) magnetic resonance imaging (MRI) technique was deemed as a promising reliable and noninvasive inspection manner. Since the first renal BOLD MRI study was reported by Prasad in 1996 [5], investigators have increasingly explored renal oxygenation principles and tissue hypoxia mechanisms. During the past two decades, many renal physiological manifestations and formation mechanisms have been elucidated. These well-accepted renal physiological discoveries were corroborated with BOLD MRI results. For example, renal tissue in the medullary zone had a lower oxygen partial pressure and hypoxia gradient than in the entire kidney parenchyma [6]. The corresponding results were obtained from renal BOLD maps analyzed by use of the concentric objects (CO) [7] and twelve-layer concentric objects (TLCO) techniques [8]. Although substantial valuable discoveries have been reported by nephrologists and radiologists worldwide, several issues have prevented BOLD MRI from extensive clinical use and have frustrated initial research enthusiasm. The first issue concerns the origin of the renal BOLD signals. It is well known that massive physicochemical or biological factors are involved in renal BOLD signal formation. These factors include regional blood oxygen supplementation, tissue oxygen consumption, hydration status, hematocrit, and salt and medicine intake [9-11]. Therefore, analysis of the BOLD signal value alone cannot determine which solitary or multiple factors are the key factors. A second problem relates to the method of renal BOLD signal analysis. Although the acquisition of renal BOLD MR images is easily performed worldwide, there is no consensus as to how to analyze the BOLD MR images. Different analysis methods could lead to significantly different results. For example, Milani et al. investigated the difference in the R2* value between patients and control subjects and did not find any difference in R2* with the use of the conventional regional ROI technique. However, significant differences in R2* values in cortical layers were revealed when the TLCO technique was adopted in the same patient cohort [8]. Overcoming these native deficiencies of BOLD MRI may assist in further understanding renal tissue oxygenation.

The main purposes of this study were to understand renal parenchyma hypoxia configuration and to develop a new BOLD image analysis method. We also compared tissue hypoxia characteristics between healthy people and patients with LN.

Methods

Study protocol

Patients

A total of forty-one participants including twenty-three patients with LN and eighteen healthy volunteers were accrued from January 2017 to June 2018. After our study protocol were examined by Tianjin Medical University General Hospital Ethical Committee and all participants have signed informed consent files, this study was authorized to carry out. Patients with lupus nephritis were diagnosed by experienced

nephrologist according to the 2012 International Collaborating Clinics classification criteria for systemic lupus erythematosus [12]. Renal functional assessment was used estimated glomerular filtration rate (eGFR) by measured serum creatinine according to Chronic Kidney Disease Epidemiology Collaboration (CKD-EPI) equation [13]. Healthy volunteers were recruited from different divisions of our hospital. Since renal oxygenation were mainly affected by oxygen supplementation and consumption, several special conditions should be avoided as much as possible. These conditions included oxygen inhalation, water or slat overload, specific medication such as diuretics, NSAIDs, vasodilators or hematopoietin

Renal histopathology

Renal biopsy specimens were made as 2-μm thick sections with histological staining. Two experienced pathologists independently diagnosed these specimens according to the ISN/RPS 2003 classification [14]. A semi-quantitative scoring system was used to assessment the pathological injuries[15].

MRI techniques

We acquired renal BOLD-MRI images by using a 3.0-T scanner (GE Discovery™ 750 3.0T; General Electric; USA). The detailed imaging parameters can be referred to our previous study [16]

Image analysis

Renal tissue oxygenation distribution was displayed by visualized R2* map by processing with FUNCTOOL program. Renal coronal anatomical plane with largest area was selected as analyzed section. The region of interest (ROI) was set as a 1 pixel (width) × 50 pixels (height) rectangle. One tip of the ROI was located on the renal cortical surface. Another tip of the ROI looked out on the renal hilus (Figure 1). R2* values of each voxel of the selected ROI were obtained with MATLAB 2014a (MathWorks Inc., Natick, MA, USA).

Statistical analyses

RM-ANOVA data

R2* values of renal BOLD maps were expressed as mean standard deviation (SD). To compare the R2* level difference between the group with LN and the control group at different depths of renal parenchyma, repeated-measures analysis of variance (RM-ANOVA) was performed. Mauchly's test was used to check whether the covariance structure satisfied the sphericity condition [17]. If the covariance matrix was satisfied with sphericity assumption, the univariate RM-ANOVA was applied for further analysis. Otherwise, multivariate ANOVA was used to analyze the data [18], and four multivariate test statistics were also calculated: Pillai's Trace statistic, Wilks' likelihood ratio, the Hotelling-Lawley Trace criterion, and Roy's Largest Root. The effects of intergroup (LN vs healthy control) and intragroup (different depths of renal parenchyma) were compared. The interaction effect was also compared. Statistical significance was accepted at $P < 0.05$. All analyses were carried out using the IBM® SPSS® Statistics software (version 22.0.0.0 IBM Corporation, Armonk, NY, USA).

Curve-fitting analysis

To describe the R2* configuration throughout the cortex and medulla, the curve-fitting analysis was selected to explore the detected R2* data. Four curve fit types (polynomial, power, exponential, and Gaussian) were chosen for data exploration. The goodness of fit was assessed with the use of multiple parameters including R^2, sum square error (ESS), and root-mean-square error (RMSE). All analyses were carried out by using the Curve Fitting Toolbox of MATLAB R2014a (MathWorks Inc.).

Results

General clinical and pathological results of patients with lupus nephritis

A total of twenty-three patients with lupus nephritis were recruited in our current study. The mean age of patients was 35.52 13.34, range from 15 to 62. The mean values of proteinuria and eGFR were 3.72 2.80 g/24h, range from 0.34 to 9.47 g/24h and 102.74 24.79 ml/min/1.73m^2, range from 39 to 138 ml/min/1.73m^2, respectively. According to the ISN/RPS 2003 classification standard, all of pathological patterns of renal biopsy were generalized three types including III, IV and V type. The detailed clinical and pathological data were showed in the Table 1. Morphology assessment results of histological injuries activity and chronicity were showed in Table 2.

Manifestation of R2* values in renal parenchyma from superficial cortex to deep medulla

According to the detection results from the rectangular ROI of BOLD MRI, we found at least two pattern categories of R2* manifestation in the renal parenchyma. The first R2* pattern in the renal parenchyma displayed two different styles, shown in the cortex and the medulla. In the

cortex or cortical–medullary conjunction zone, the increment of R2* values concomitant with increasing depth renal parenchyma was slight, fluctuating in a small range. However, a conspicuous uptrend of R2* values was observed in the deeper medulla zone. Compared with the correlation between R2* values and renal depth of parenchyma, the slope of R2* values in the deeper medulla zone was steeper than that in the cortex zone. We call this pattern of R2* values the "sharp uptrend style." The second R2* pattern in kidneys was different from the first pattern. The R2* values maintained a relatively stable level throughout the cortical and medullary zones. We call this pattern of R2* values the "flat uptrend style" (Figure 2). Based on these findings, we provided the definition of two styles of R2* values. If the highest R2* value exceeded 100% increasing magnitude of lowest R2* value, this sample was classified as sharp uptrend style. Correspondingly, if the highest R2* value did not exceed 25% increasing magnitude of lowest R2* value, this sample was classified as flat uptrend style.

Analysis of two patterns of R2* values shows a difference between patients with LN and healthy volunteers

In order to analyze two styles of R2* values in renal parenchyma, the extreme R2* data including highest R2* average values with maximal range and lowest R2* average values with minimal range were selected from each study subject. We selected 8 clusters highest extreme R2* data and 8 clusters lowest extreme R2* data in each research subject. Because the height of the rectangular ROI was 50 pixels, we divided the renal parenchyma into 50 layers. The average R2* values in each renal parenchyma layers are shown in Figure 3.

There was a very small difference in the R2 value curves between the LN group and the control group when the depth of renal parenchyma was less than 25 layers. However, the slope of the R2* curve in the LN group was lower than that in the control group at a depth of 25-50 renal layers. We compared the sharp uptrend style pattern of R2* values in both the LN group and the control group by using RM-ANOVA. Because Mauchly's test showed that covariance structure was not satisfied with sphericity assumption ($P < 0.001$), multivariate ANOVA was chosen for further data. The statistical difference in R2* values between renal parenchyma layers was observed in both the LN group and the healthy volunteer group (Pillai's Trace statistic, $P < 0.001$; Wilks' likelihood ratio, $P < 0.001$; Hotelling-Lawley Trace criterion, $P < 0.001$; Roy's Largest Root, $P < 0.001$). The statistical interaction effect between renal parenchyma layers and study groups was also observed (Pillai's Trace statistic, $P = 0.004$; Wilks' likelihood ratio, $P = 0.004$; Hotelling-Lawley Trace criterion, $P = 0.004$; Roy's Largest Root, $P = 0.004$).

Similar results were found for the flat uptrend style pattern of R2* data. In the superficial zone of renal parenchyma (less than 25 layers), the location of the R2* curve in the LN group was lower than that in the control group. However, the difference in R2* values in the deep medullary zone was not distinct. RM-ANOVA results showed a statistic difference between the two R2* curves. Multivariate ANOVA was used again because of the similar Mauchly's test results. Both difference in renal parenchyma layers and interaction effect with study groups showed statistical significance (Pillai's Trace statistic, $P < 0.001$; Wilks' likelihood ratio, $P < 0.001$; Hotelling-Lawley Trace criterion, $P < 0.001$; Roy's Largest Root, $P < 0.001$) (see Figure 3).

Comparison of R2* data goodness of fit by multiple mathematic function models

We collected several sets of R2* data from the renal parenchyma in both patients with LN and healthy volunteers. Four categories of mathematic functions (polynomial, power, exponential, and Gaussian functions) were used to fit virtual R2* data. By comparison with goodness of fit indexes, the Gaussian functional model was recognized as the best-fit model for both sharp uptrend style data or flat uptrend style data. Goodness of fit indexes for the four mathematic functional models are listed in Tables 3 and 4. The fit curves of these models are displayed in Figure 4.

Discussion

One of the primary aims was to understand the relationship between tissue oxygenation and renal parenchyma depth. Our current study revealed two categories of renal oxygenation manifestation patterns. One pattern, the sharp uptrend style, has better tissue oxygenation with a slight fluctuation in the superficial layers of the kidney. Subsequently, a sharp increment of deoxygenation was observed in the deep layers of the renal parenchyma. Although this pattern has similar characteristics with the well-known renal tissue oxygenation feature, such as higher deoxygenation in the medulla than in the cortex [19], a distinct two-phase oxygenation feature was different from that in many previous studies [20-22]. This sharp uptrend style of renal R2* values might correlate with a sophisticated relationship between tissue partial pressure of oxygen (PaO_2) and oxyhemoglobin saturation dissociation curve. Tissue oxyhemoglobin saturation could be maintained in a stabilized level when PaO_2 is above 60 mmHg, whereas there is a steep gradient with a sharp decrease in oxyhemoglobin when the PaO_2 is less than 26.6 mmHg. Previous research has shown that PaO_2 in the majority of cortexes is usually higher than 60 mmHg, whereas medullary PaO_2 rarely exceeds 26.6 mmHg [23]. Another relevant reason was interrelated with 2,3-diphosphoglycerate (DPG)-mediated oxyhemoglobin affinity. A lessening in oxyhemoglobin affinity has been deemed as an important physiological adaptive response to conditions in which oxygen delivery is impaired. The increased oxyhemoglobin affinity may actually impair tissue oxygenation [24]. Moreover, another pattern of R2* values, the flat uptrend style, was also found in our current study. We found that the R2* values fluctuated in a narrow range throughout the depth of renal parenchyma. R2* values in the deep medulla were only slightly higher than those in the superficial cortex. We even found no

discrepancy in R2* level between the superficial renal zone and the deep renal zone, in sporadic samples. This phenomenon implies that tissue oxygenation in the deep medullary zone is not always lower than that in the superficial cortical zone. This discovery is a challenge to the recognized opinion that had been testified by many studies.

Unfortunately, we could not detect renal parenchyma histological and cellular physiological conditions simultaneously. The potential explanation of these two patterns was only based on reasonable ratiocination. In renal cortical zone, the oxygen tension is more variable because of the fluctuation of renal blood perfusion. The existence of an arterial-to-venous oxygen shunt mechanism can maintain the average partial pressure of oxygen (pO2) at approximately 30 mmHg. Schurek et al and Welch et al verified that oxygen tension in renal vein exceeded that in glomerular capillaries and that in the efferent arteriole, respectively [25, 26]. These findings confirmed the existence of oxygen shunt, which was the renal oxygenation homeostatic mechanism. The arterial-to-venous oxygen shunt mechanism maybe one of reasons why deoxyhemoglobin can be detected in the well blood perfusion cortical zone. However, the oxygen supplement in medullary zone was obvious lower than that in cortical zone, not to mention high local oxygen consumption for tubular reabsorption. Other compensative mechanisms such as prostaglandins, nitric oxide (NO), and adenosine were involved. These compensative mechanisms continuously adjust medullary tubular transport activity to the limited available oxygen supply, acting by both enhancement of regional blood flow and downregulation of distal tubular transport, particularly in medullary thick ascending limbs (mTAL) [23]. We speculated the gradient of deoxyhemoglobin in medulla perhaps preserved at similar level in cortex. On the other hand, another pattern of R2* value called “sharp uptrend style” could be also found. It was implied that the quantity of deoxyhemoglobin increased significantly. This R2* values manifestation was observed not only in patients with lupus nephritis but also in healthy volunteers. We speculated several possible pathophysiological mechanisms were involved. Firstly, glomerular hyperfiltration is one condition that increases oxygen demand in renal parenchyma. When glomerular filtration rate is exorbitance, more plasma is also filter out. This condition results in sodium overload in tubular lumen and requires more energy for the reabsorption of sodium by tubular cells[27]. Secondly, oxidative stress can result tissue hypoxia by superoxide radicals decreasing the bioavailability of nitric oxide. Reduced tissue nitric oxide leads to vasoconstriction and decrease in regional blood flow. Furthermore, increased oxidative stress can evaluate oxygen consumption in kidney, possibly via the effects on tubular transporters [28, 29]. Thirdly, loss of peritubular capillaries or reduction in peritubular capillary flow may give raise to renal hypoxia. Previous studies on animal models have showed that tubulointerstitial injury is associated with the distortion and loss of peritubular capillaries[30]. Activation of renin-angiotensin system (RAS) and imbalance of vasoactive substances lead to vasoconstriction and lessen peritubular capillary flow[27].

Our current findings were different from both earlier BOLD MRI studies and direct measurement of tissue oxygen levels with oxygen electrodes animal studies. Our current study found that not all samples from deep medulla showed significant higher R2* values. Compared with R2* values in cortical zone, similar R2* values were detected by BOLD-MRI in deep medullary zone. Moreover, this quaint phenomenon displayed in both patients with LN and healthy controls. It seemed that deep medullary zone had also well oxygenation. This specious deduction contradicted with results for renal oxygenation detected by microelectrode in many previous animal investigations [31, 32]. It seemed dogmatic that higher tissue oxygenation was also found in deep medullary zone according to our observation. In evaluation renal oxygenation status, four kinds of methods were usually applied. (1) measurement of oxidative ability of oxygen molecules, usually by microelectrode. (2) detection the ratio of oxyhemoglobin/total hemoglobin. (3) detection of HIF activity. (4) measurement the magnitude of oxygen molecules in renal parenchyma. Previous animal studies proved difference of oxygen partial pressure between renal cortex and renal medulla. Results in these investigations were obtained by microelectrode in general. BOLD-MRI technique applied R2* values as oxygenation sensor. R2* values which is called spin-spin relaxation rate reflects the deoxyhemoglobin concentration in local tissues. The amount of R2* values dependent on local deoxyhemoglobin concentration rather than local oxygen partial pressure. For example, when renal tissues suffered from anemia, the amount of hemoglobin or deoxyhemoglobin may frequently change. Whereas, the partial pressure of oxygen usually keeps stable state. So, our study team speculated that there was a possibility which ostensible results could be found by BOLD-MRI and microelectrode simultaneously. On the other hand, results of deoxyhemoglobin concentration-based method were influenced by multiple factors such as local blood flow supplementation, changes in pH, acid-base disorder, micro-environmental changes (Bohr effect), oxygen shunt between renal arterial and venous, etc [5, 33]. Our research team speculated one or several mechanisms gave rise to lower deoxyhemoglobin in deep medulla. This may partially interpret why corticomedullary gradient of oxygenation is not observed by R2* index. In order to testify our speculation, another MRI-based technique called relaxation rate of the T1 signal (R1) can be applied, which may correlate with oxygen molecules itself, although it is less sensitive in detecting renal hypoxia than R2*-based technique [34].

Another result of our study involved exploring the possibility of describing renal parenchyma R2* patterns by mathematic models. Some investigators thought that the renal tissue oxygenation status was influenced by multiple factors, such as local blood supplementation and tissue oxygen consumption. Therefore, detected R2* values in each pixel from anywhere in the BOLD images were always the integrated results of multiple physiological factors. The key problem was that the precise participation proportion of each factor was not well understood. However, we believed that information on all involved physiological factors with similar to the encrypted message was still sealed in these R2* maps. We still hope to unlock this sealed information with the right decoding method. By testing the multiple mathematic functions, we found that Gaussian function had the best capability to fit practical R2* data. Moreover, both the sharp uptrend style data and the flat uptrend style

data fit the Gaussian function well with two or more compartments. Although there was no reliable evidence to verify the corresponding relationship between renal biological factors and compartments of fit Gaussian functions, we hypothesized that those multiple encrypted and perplexing physiological messages in the R2* data could be transformed into another mode. Perhaps we will decode the encrypted biological messages that were composed in R2* data by studying fit Gaussian functions.

Our study also compared renal histological data with R2* values. In proliferative LN such as type III or type IV, lower renal tissue R2* values usually correspond with severe tubular damage. The inverse manifestation was observed in non-proliferative LN in which mild tubular injuries could be confirmed with renal biopsy samples [35]. Despite statistical discrepancy of R2* values detected between the two groups in both sharp uptrend and flat uptrend style data, the substantial R2* difference was very small. We speculated that at least two factors were involved and that the pathogenesis was similar to that in patients with renal artery stenosis. Hansell et al. found that kidneys usually had increased renal blood flow instead of regional pO2 when the renal parenchyma was under severe hypoxia conditions. The increased renal blood flow also led to GFR increments that subsequently induced more filtered sodium in the renal tubules. The reinforced tubular sodium reabsorption was the main reason for increased oxygen consumption [36]. Due to R2* values indicated magnitude of deoxyhemoglobin according to the principle of BOLD imaging, lower R2* in cortex implied the better cortical oxygenation. Morphology assessment of renal biopsy samples showed tubulointerstitial inflammation or atrophy could be been in patients with proliferative lupus nephritis. We speculated these pathological injuries might weaken tubular transport activity, which subsequently reduced oxygen consumption and decreased the R2* values. Our surmise was also confirmed by our previous study. Furthermore, faded GFR also led to downward R2* due to lessened solute delivery for tubular transport. These possible mechanisms listed above might explain the tendency of R2* in Figure 3 that both crossover of two R2* curves in medulla and separation of two R2* curves in cortex could be detected simultaneously. Our research team also considered that the integrity of renal physiological function in healthy volunteers was superior to that in patients with lupus nephritis. The preserved glomerular and tubulointerstitial construction and function were prone to oxygen consumption, and integrate peritubular capillary would transport more hemoglobin into renal tissues. We speculated that this was one of the reasons why higher R2* values were found at deep medullary zone in sharp upturn style and superficial cortical zone in flat upturn style.

We also developed a novel ROI method called the “narrow rectangle” or “virtual probe” to measure renal R2* values. This was the principal reason why we devised and applied this special ROI technique. Renal microstructure displays distinct directional characteristics and spatial heterogeneity. Renal parenchyma oxygenation features are based on its histological anatomy foundation. The well-known opinion that the degree of renal blood oxygen saturation in the cortical zone is always higher than that in the medullary zone is based on previous ROI analysis methods such as regional ROI selection [37], compartmental approach [38], fractional kidney hypoxia [39], CO [7], and TLCO [8]. However, investigators either handled nonconsecutive crude R2* data by regional ROI selection or acquired calculated mean R2* results by CO and TLCO methods. These inherent shortcomings remained an obstacle to the procurement of the explicit oxygenation tendency throughout the renal parenchyma. Contrary to previous conventional ROI analysis methods, our new analysis technique revealed that deep medullary oxygenation was not always overtly lower than cortical oxygenation. This unusual discovery challenged the well-known opinion.

Our current study still had several shortcomings. First, our study merely investigated renal R2* signal instead of other functional MR signals such as ADC, synchronously. We only knew the existing oxygenation condition, whereas we did not understand the precise mechanism of hypoxia status formation. Second, the meaning of fitted Gaussian functions had not yet been explained or proved by other physiological studies, and we only hypothesized that fitted Gaussian formulas represent renal hypoxia outline in the kidney cortical and medullary zones. Third, the narrow rectangular ROI analysis method that was adopted in our study had not been tested by many researchers. Because the highly observer-dependent property of previous conventional ROI analysis methods has been proved, we did not know the new ROI analysis technique had the highly reproducible and lower variant characteristic.

Conclusions

Renal medullary oxygenation status detected by BOLD signals can vary remarkably. Although BOLD-MRI provides a non-invasive way to explore renal oxygenation, the comprehensive recognition in renal hypoxia should induct multiple assessment methods simultaneously. BOLD-MRI signal patterns from renal parenchyma could be described by the Gaussian function model. Understanding renal parenchyma deoxyhemoglobin distribution patterns may be helpful to recognize the principle of renal hypoxia.

Abbreviations

Blood oxygen level dependent, **BOLD**; Chronic Kidney Disease Epidemiology Collaboration ,**CKD-EPI**; Concentric objects, **CO**; Field of view, **FOV**; Functional magnetic resonance imaging, **fMRI**; Lupus nephritis, **LN**; Magnetic resonance imaging, **MRI**; Region of interest, **ROI**; Repeated-measures analysis of variance, **RM-ANOVA**; Root-mean-square error, **RMSE**; Systemic lupus erythematosus, **SLE**; SLE Disease Activity Index, **SLEDAI**; Spoiled gradient recalled echo, **SPGR**; Sum square error, **ESS**; Twelve-layer concentric objects, **TLCO**; Repetition time, **TR**; Echo time, **TE**;

Declarations

Ethics approval and consent to participate

This study was approved by the ethics committee of Tianjin Medical University General Hospital prior to the commencement of the study. Written informed consent for participation was obtained from the patient or a legal representative.

Consent for publication

Not applicable

Availability of data and material

The datasets used and/or analyzed during the current study are available from the corresponding author on reasonable request.

Competing interests

The authors declare that they have no competing interests.

Funding

No funding

Authors' contributions

ZFZ and YYW are the guarantors of integrity of the entire study and are also responsible for study concepts and design. HLS and TKY are in charge of MR imaging, data analysis and manuscript drafting. JYJ and DL are responsible for renal clinical data. LW and WYS are responsible for renal biopsy and pathological diagnosis. We confirm that all the listed authors have participated actively in the study, and have seen and approved the submitted manuscript.

Acknowledgements

We thank LetPub (www.letpub.com) for its linguistic assistance during the preparation of this manuscript.

References

1. Pan Q, Li Y, Ye L, Deng Z, Li L, Feng Y, Liu W, Liu H: **Geographical distribution, a risk factor for the incidence of lupus nephritis in China**. *BMC Nephrol* 2014, **15**:67.
2. Austin HA, 3rd, Boumpas DT, Vaughan EM, Balow JE: **Predicting renal outcomes in severe lupus nephritis: contributions of clinical and histologic data**. *Kidney Int* 1994, **45**(2):544-550.
3. Bihl GR, Petri M, Fine DM: **Kidney biopsy in lupus nephritis: look before you leap**. *Nephrol Dial Transplant* 2006, **21**(7):1749-1752.
4. Corapi KM, Chen JL, Balk EM, Gordon CE: **Bleeding complications of native kidney biopsy: a systematic review and meta-analysis**. *Am J Kidney Dis* 2012, **60**(1):62-73.
5. Prasad PV, Edelman RR, Epstein FH: **Noninvasive evaluation of intrarenal oxygenation with BOLD MRI**. *Circulation* 1996, **94**(12):3271-3275.
6. Pallone TL, Robertson CR, Jamison RL: **Renal medullary microcirculation**. *Physiol Rev* 1990, **70**(3):885-920.
7. Piskunowicz M, Hofmann L, Zuercher E, Bassi I, Milani B, Stuber M, Narkiewicz K, Vogt B, Burnier M, Pruijm M: **A new technique with high reproducibility to estimate renal oxygenation using BOLD-MRI in chronic kidney disease**. *Magn Reson Imaging* 2015, **33**(3):253-261.
8. Milani B, Ansaloni A, Sousa-Guimaraes S, Vakilzadeh N, Piskunowicz M, Vogt B, Stuber M, Burnier M, Pruijm M: **Reduction of cortical oxygenation in chronic kidney disease: evidence obtained with a new analysis method of blood oxygenation level-dependent magnetic resonance imaging**. *Nephrol Dial Transplant* 2017, **32**(12):2097-2105.
9. Prasad PV, Epstein FH: **Changes in renal medullary pO2 during water diuresis as evaluated by blood oxygenation level-dependent magnetic resonance imaging: effects of aging and cyclooxygenase inhibition**. *Kidney Int* 1999, **55**(1):294-298.
10. Pruijm M, Hofmann L, Maillard M, Tremblay S, Glatz N, Wuerzner G, Burnier M, Vogt B: **Effect of sodium loading/depletion on renal oxygenation in young normotensive and hypertensive men**. *Hypertension* 2010, **55**(5):1116-1122.
11. Neugarten J: **Renal BOLD-MRI and assessment for renal hypoxia**. *Kidney Int* 2012, **81**(7):613-614.

12. Petri M, Orbai AM, Alarcon GS, Gordon C, Merrill JT, Fortin PR, Bruce IN, Isenberg D, Wallace DJ, Nived O *et al*: **Derivation and validation of the Systemic Lupus International Collaborating Clinics classification criteria for systemic lupus erythematosus**. *Arthritis Rheum* 2012, **64**(8):2677-2686.
13. Levey AS, Stevens LA, Schmid CH, Zhang YL, Castro AF, 3rd, Feldman HI, Kusek JW, Eggers P, Van Lente F, Greene T *et al*: **A new equation to estimate glomerular filtration rate**. *Ann Intern Med* 2009, **150**(9):604-612.
14. Weening JJ, D'Agati VD, Schwartz MM, Seshan SV, Alpers CE, Appel GB, Balow JE, Bruijn JA, Cook T, Ferrario F *et al*: **The classification of glomerulonephritis in systemic lupus erythematosus revisited**. *Kidney Int* 2004, **65**(2):521-530.
15. Austin HA, 3rd, Muenz LR, Joyce KM, Antonovych TT, Balow JE: **Diffuse proliferative lupus nephritis: identification of specific pathologic features affecting renal outcome**. *Kidney Int* 1984, **25**(4):689-695.
16. Shi H, Jia J, Li D, Wei L, Shang W, Zheng Z: **Blood oxygen level dependent magnetic resonance imaging for detecting pathological patterns in lupus nephritis patients: a preliminary study using a decision tree model**. *BMC Nephrol* 2018, **19**(1):33.
17. Park E, Cho M, Ki CS: **Correct use of repeated measures analysis of variance**. *Korean J Lab Med* 2009, **29**(1):1-9.
18. Maurissen JP, Vidmar TJ: **Repeated-measure analyses: Which one? A survey of statistical models and recommendations for reporting**. *Neurotoxicol Teratol* 2017, **59**:78-84.
19. Zheng Z, Shi H, Ma H, Li F, Zhang J, Zhang Y: **Renal Oxygenation Characteristics in Healthy Native Kidneys: Assessment with Blood Oxygen Level-Dependent Magnetic Resonance Imaging**. *Nephron Physiol* 2014, **128**(3-4):47-54.
20. Gloviczki ML, Glockner JF, Crane JA, McKusick MA, Misra S, Grande JP, Lerman LO, Textor SC: **Blood oxygen level-dependent magnetic resonance imaging identifies cortical hypoxia in severe renovascular disease**. *Hypertension* 2011, **58**(6):1066-1072.
21. Yin WJ, Liu F, Li XM, Yang L, Zhao S, Huang ZX, Huang YQ, Liu RB: **Noninvasive evaluation of renal oxygenation in diabetic nephropathy by BOLD-MRI**. *Eur J Radiol* 2012, **81**(7):1426-1431.
22. Xin-Long P, Jing-Xia X, Jian-Yu L, Song W, Xin-Kui T: **A preliminary study of blood-oxygen-level-dependent MRI in patients with chronic kidney disease**. *Magn Reson Imaging* 2012, **30**(3):330-335.
23. Brezis M, Rosen S: **Hypoxia of the renal medulla--its implications for disease**. *N Engl J Med* 1995, **332**(10):647-655.
24. Riggs TE, Shafer AW, Guenter CA: **Acute changes in oxyhemoglobin affinity. Effects on oxygen transport and utilization**. *J Clin Invest* 1973, **52**(10):2660-2663.
25. Schurek HJ, Jost U, Baumgartl H, Bertram H, Heckmann U: **Evidence for a preglomerular oxygen diffusion shunt in rat renal cortex**. *Am J Physiol* 1990, **259**(6 Pt 2):F910-915.
26. Welch WJ, Baumgartl H, Lubbers D, Wilcox CS: **Nephron pO2 and renal oxygen usage in the hypertensive rat kidney**. *Kidney Int* 2001, **59**(1):230-237.
27. Korner A, Eklof AC, Celsi G, Aperia A: **Increased renal metabolism in diabetes. Mechanism and functional implications**. *Diabetes* 1994, **43**(5):629-633.
28. Katavetin P, Miyata T, Inagi R, Tanaka T, Sassa R, Ingelfinger JR, Fujita T, Nangaku M: **High glucose blunts vascular endothelial growth factor response to hypoxia via the oxidative stress-regulated hypoxia-inducible factor/hypoxia-responsible element pathway**. *J Am Soc Nephrol* 2006, **17**(5):1405-1413.
29. Banday AA, Lokhandwala MF: **Oxidative stress-induced renal angiotensin AT1 receptor upregulation causes increased stimulation of sodium transporters and hypertension**. *Am J Physiol Renal Physiol* 2008, **295**(3):F698-706.
30. Ohashi R, Shimizu A, Masuda Y, Kitamura H, Ishizaki M, Sugisaki Y, Yamanaka N: **Peritubular capillary regression during the progression of experimental obstructive nephropathy**. *J Am Soc Nephrol* 2002, **13**(7):1795-1805.
31. Friederich-Persson M, Thorn E, Hansell P, Nangaku M, Levin M, Palm F: **Kidney hypoxia, attributable to increased oxygen consumption, induces nephropathy independently of hyperglycemia and oxidative stress**. *Hypertension* 2013, **62**(5):914-919.
32. Nordquist L, Friederich-Persson M, Fasching A, Liss P, Shoji K, Nangaku M, Hansell P, Palm F: **Activation of hypoxia-inducible factors prevents diabetic nephropathy**. *J Am Soc Nephrol* 2015, **26**(2):328-338.
33. Prasad PV: **Evaluation of intra-renal oxygenation by BOLD MRI**. *Nephron Clin Pract* 2006, **103**(2):c58-65.
34. Winter JD, Estrada M, Cheng HL: **Normal tissue quantitative T1 and T2* MRI relaxation time responses to hypercapnic and hyperoxic gases**. *Acad Radiol* 2011, **18**(9):1159-1167.
35. Shi H, Yan T, Li D, Jia J, Shang W, Wei L, Zheng Z: **Detection of Renal Hypoxia in Lupus Nephritis Using Blood Oxygen Level-Dependent MR Imaging: A Multiple Correspondence Analysis**. *Kidney Blood Press Res* 2017, **42**(1):123-135.
36. Hansell P, Welch WJ, Blantz RC, Palm F: **Determinants of kidney oxygen consumption and their relationship to tissue oxygen tension in diabetes and hypertension**. *Clin Exp Pharmacol Physiol* 2013, **40**(2):123-137.

37. Khatir DS, Pedersen M, Jespersen B, Buus NH: **Evaluation of Renal Blood Flow and Oxygenation in CKD Using Magnetic Resonance Imaging**. *Am J Kidney Dis* 2015, **66**(3):402-411.
38. Ebrahimi B, Gloviczki M, Woollard JR, Crane JA, Textor SC, Lerman LO: **Compartmental analysis of renal BOLD MRI data: introduction and validation**. *Invest Radiol* 2012, **47**(3):175-182.
39. Saad A, Crane J, Glockner JF, Herrmann SM, Friedman H, Ebrahimi B, Lerman LO, Textor SC: **Human renovascular disease: estimating fractional tissue hypoxia to analyze blood oxygen level-dependent MR**. *Radiology* 2013, **268**(3):770-778.

Tables

Table 1: Baseline clinical and pathological data of patents with lupus nephritis.

Case number	Age (year)	Gender	Proteinuria (g/24h)	eGFR (ml/min/1.73m^2)	Pathological diagnosis
1	32	female	4.76	62	IV-G(A/C)+V
2	30	female	6.44	138	V
3	51	female	2.14	98	III-(A/C)
4	48	male	9.47	71	IV-S(A/C)+V
5	15	female	1.87	39	IV-S(A/C)
6	36	female	4.63	131	IV-G(A/C)+V
7	43	female	0.34	113	IV-G(A/C)+V
8	23	female	1.15	113	III-(A/C)+V
9	18	female	0.81	120	III-(A/C)
10	24	male	0.58	123	III-(A/C)
11	41	female	5.81	89	IV-S(A)
12	28	female	1.57	138	V
13	20	female	1.46	105	IV-G(A/C)
14	30	female	1.34	118	V
15	62	female	5.2	85	V
16	52	female	2.08	82	IV-S(A/C)
17	31	female	2.08	80	III-(A/C)
18	22	female	6.51	124	III-(A/C)+V
19	45	female	0.58	118	IV-G(A/C)
20	28	female	6.79	98	IV-G(A/C)+V
21	60	female	8.25	97	V
22	46	female	4.67	113	IV-G(A/C)
23	32	female	7.14	108	III-(A/C)+V

Table 2: Comparisons of renal pathological parameter scores in 23 patients with lupus nephritis.

Light microscopy	Case 1	Case 2	Case 3	Case 4	Case 5	Case 6	Case 7	Case 8	Case 9	Case 10	Case 11	Case 12	Case 13	Case 14	Case 15	Case 16	Case 17	Case 18	Case 19	Case 20	Case 21	Case 22	Case 23
Number of glomeruli	14	28	41	16	21	16	17	27	21	15	15	21	18	22	25	17	32	26	14	15	14	21	27
Activity Index (AI)																							
Glomerular cell proliferation	2	0	2	2	1	1	2	1	1	2	2	0	2	0	0	2	1	1	2	2	0	1	1
Leucocyte exudation	1	0	1	2	2	2	2	2	0	1	1	0	0	0	0	1	1	1	2	2	0	2	1
Karyorrhexis and fibrinoid necrosis	1	0	1	0	1	1	1	1	0	0	1	0	1	0	0	0	0	0	1	2	0	1	0
Cellular crescents	2	0	1	2	1	3	1	1	1	1	1	0	2	0	0	1	0	1	2	2	0	1	1
Hyaline deposits	1	0	1	2	2	1	2	1	1	1	2	1	1	0	1	1	1	1	2	1	1	1	1
Interstitial inflammation	2	1	1	1	1	2	1	1	1	1	2	1	1	1	1	2	1	2	1	1	1	2	1
AI score	12	1	9	11	10	14	11	9	5	7	11	2	10	1	2	8	4	7	13	14	2	10	6
Chronicity Index (CI)																							
Glomerular sclerosis	1	0	1	0	1	0	1	1	1	0	0	1	0	0	1	0	0	1	1	0	1	1	0
Fibrous crescents	1	0	0	1	0	2	0	0	0	0	0	0	1	0	0	1	0	0	1	1	0	1	0
Tubular atrophy	2	1	1	2	1	1	1	1	1	1	0	0	1	1	0	2	1	2	2	2	0	2	1
Interstitial fibrosis	1	1	1	1	1	2	1	1	1	1	1	1	1	0	0	1	1	1	1	1	1	1	1
CI score	5	2	3	4	3	5	3	3	3	2	1	2	3	1	1	4	2	4	5	4	2	5	2
Pathological diagnosis	IV+V	V	III	IV+V	IV	IV+V	IV+V	III+V	III	III	IV	V	IV	V	V	IV	III	III+V	IV	IV+V	V	IV	III+V

Note: AI was defined as the sum of individual scores of activity items including glomerular proliferation, leucocyte exudation, karyorrhexis/fibrinoid necrosis (Í2), cellular crescents (Í2), hyaline deposits, and interstitial inflammation. The maximum score was 24 points for AI. CI was defined as chronicity items including glomerular sclerosis, fibrous crescents, tubular atrophy, and interstitial fibrosis. The maximum score was 12 points of the CI.

Table 3: Goodness of fit curve parameters in four mathematic functions in the healthy volunteer group

Category of fitted functions	Fitted parameters in sharp uptrend style R2* data			Fitted parameters in flat uptrend style R2* data		
	SSE	RMSE	R^2	SSE	RMSE	R^2
Polynomial formula	2364.000	7.093	0.587	2608.400	7.372	0.175
Power formula	587.996	3.537	0.897	2063.900	6.557	0.347
Exponential formula	175.537	1.954	0.969	687.032	3.823	0.783
Gaussian formula	24.643	0.748	0.995	14.078	0.559	0.996

Note: SSE, sum square error; RMSE, root-mean-square error.

Table 4: Goodness of fit curve parameters in four mathematic functions in the LN group

Category of fitted functions	Fitted parameters in sharp uptrend style R2* data			Fitted parameters in flat uptrend style R2* data		
	SSE	RMSE	R^2	SSE	RMSE	R^2
Polynomial formula	1385.400	5.429	0.787	2753.900	7.575	0.152
Power formula	198.665	2.056	0.970	2314.800	6.945	0.287
Exponential formula	181.703	1.988	0.972	1015.600	4.649	0.687
Gaussian formula	35.706	0.901	0.995	430.817	3.094	0.867

Note: SSE, sum square error; RMSE, root-mean-square error.

Figures

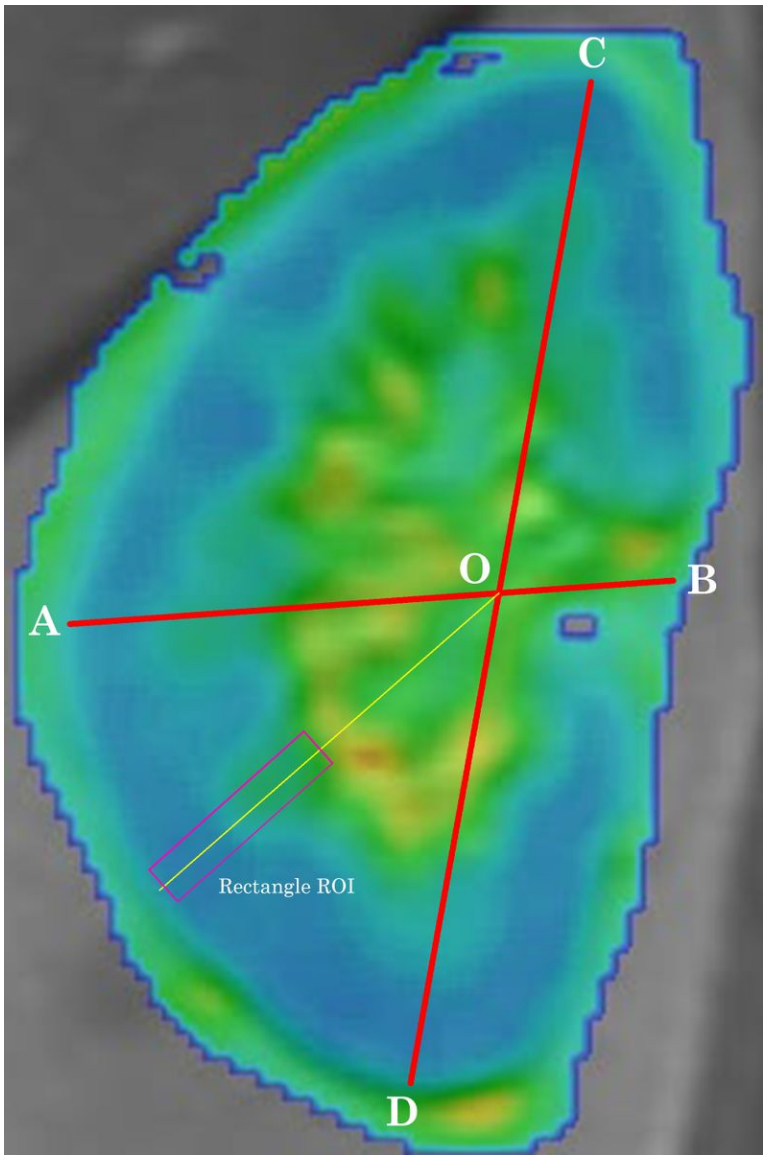

Figure 1

The way the rectangular ROI was used in the renal R2* map. This coronal section of the renal R2* map came from the left kidney of a patient with LN. The line AB linked the renal middle pole and the renal hilus. The line CD was connected between the renal upper pole and the lower pole. Point O was the junction of the two lines. In order to acquire the consecutive R2* data along the direction from the superficial cortex to

the deep layer medulla, the rectangular ROI was placed in the renal parenchyma BOLD imaging. One tip of the ROI was located on the renal cortical surface. Another tip of the ROI looked out on the point O. The long axis of the rectangular ROI is shown by the yellow line.

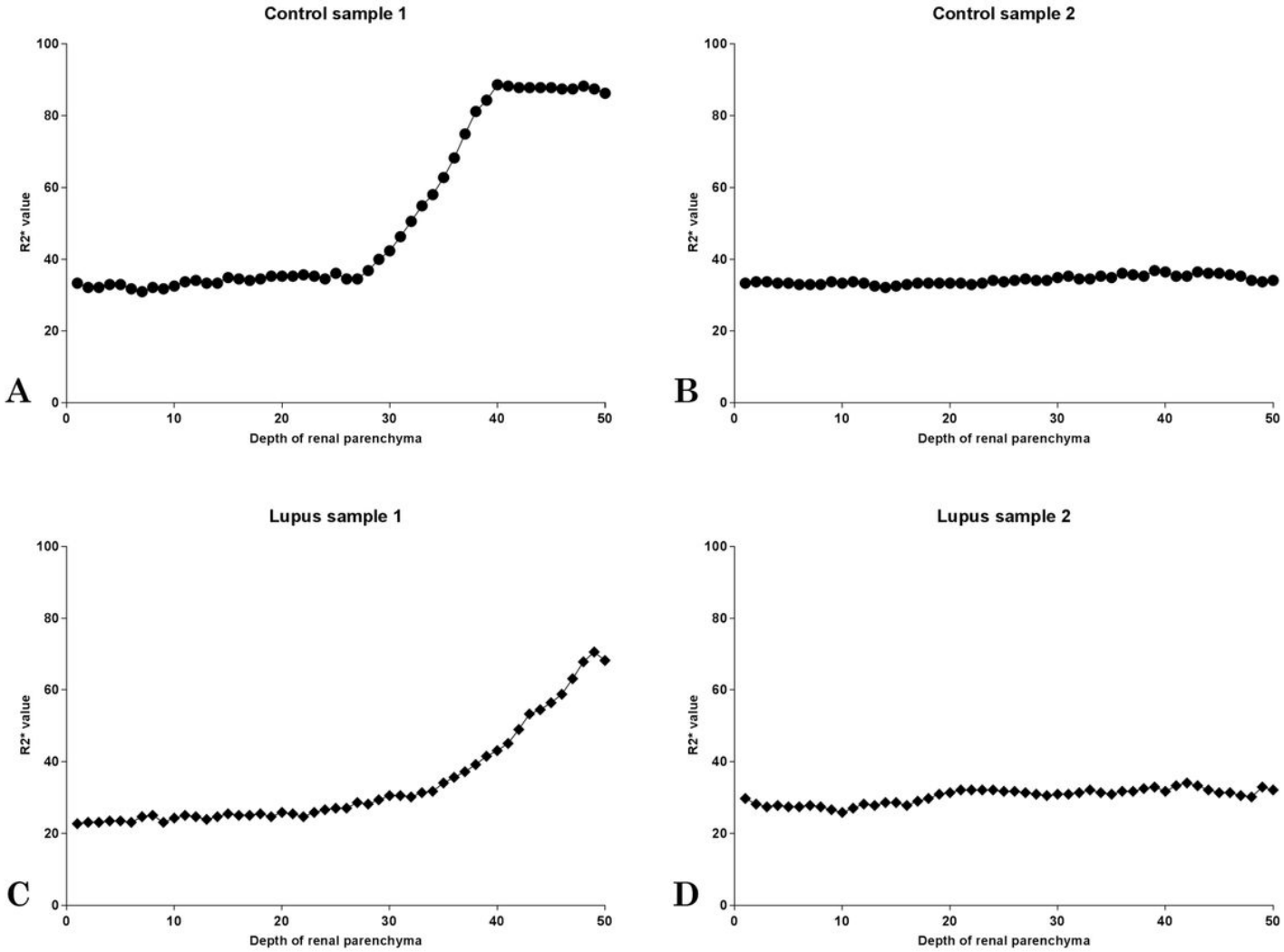

Figure 2

Manifestation of R2* value from the superficial cortex to the deep medulla. We detected four samples of R2* values from one healthy volunteer (A and B) and one patient with LN (C and D). A and C, One pattern of R2* values manifestation. R2* values in the superficial cortex fluctuated in a slight magnitude, and we observed only a very small increment of R2*. However, a remarkable R2* value augmentation was detected in the deep medullary part. B and D. Another pattern of R2* values representation in which the R2* values maintained a stabilized level throughout the depth of the renal parenchyma.

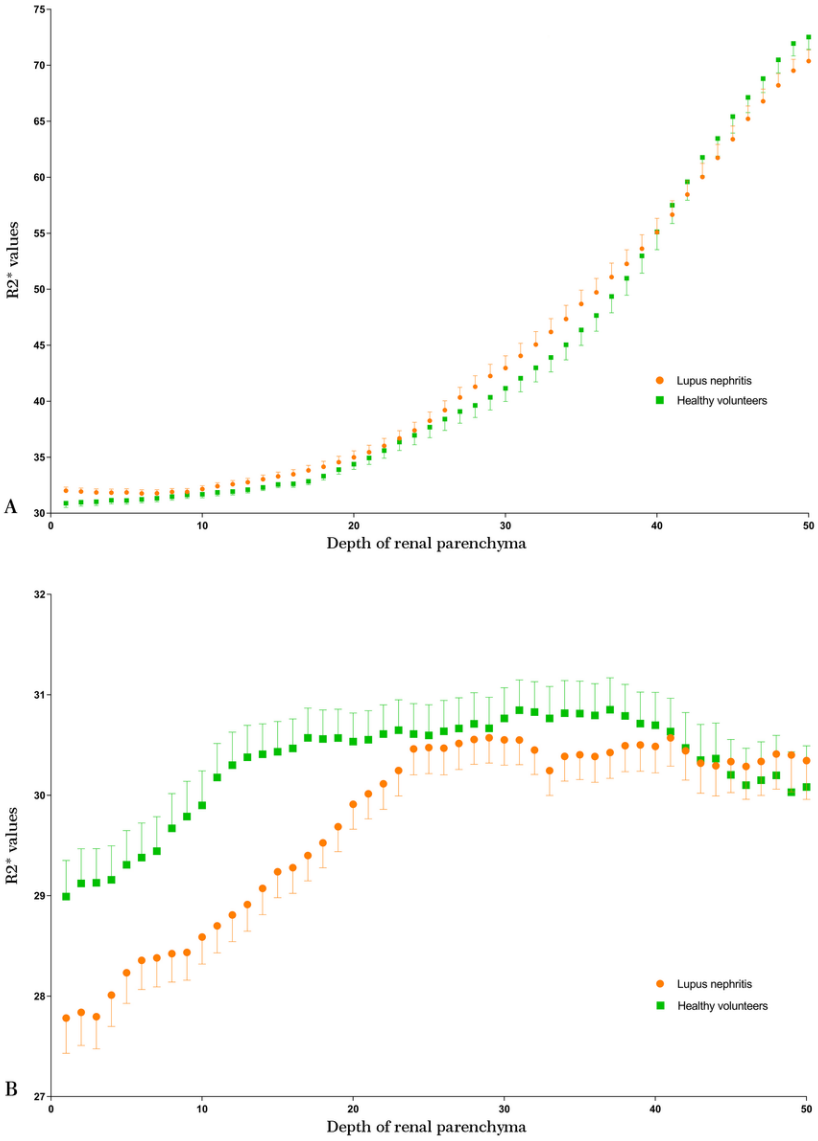

Figure 3

Comparison of the tendency of R2* values between patients with LN and healthy volunteers. Orange points and green squares indicate R2* data for patients with LN and healthy volunteers, respectively. A, Comparison result of R2* data in a sharply raising style. R2* values of patients with LN are slightly higher than those for healthy volunteers in the cortical zone. The tendency reversed in the deep medullary zone. B, Comparison result of R2* data in a slowly raising style. R2* values for patients with LN are slightly lower than those of healthy volunteers in the cortical zone. No distinct difference was found in the deep medullary zone.

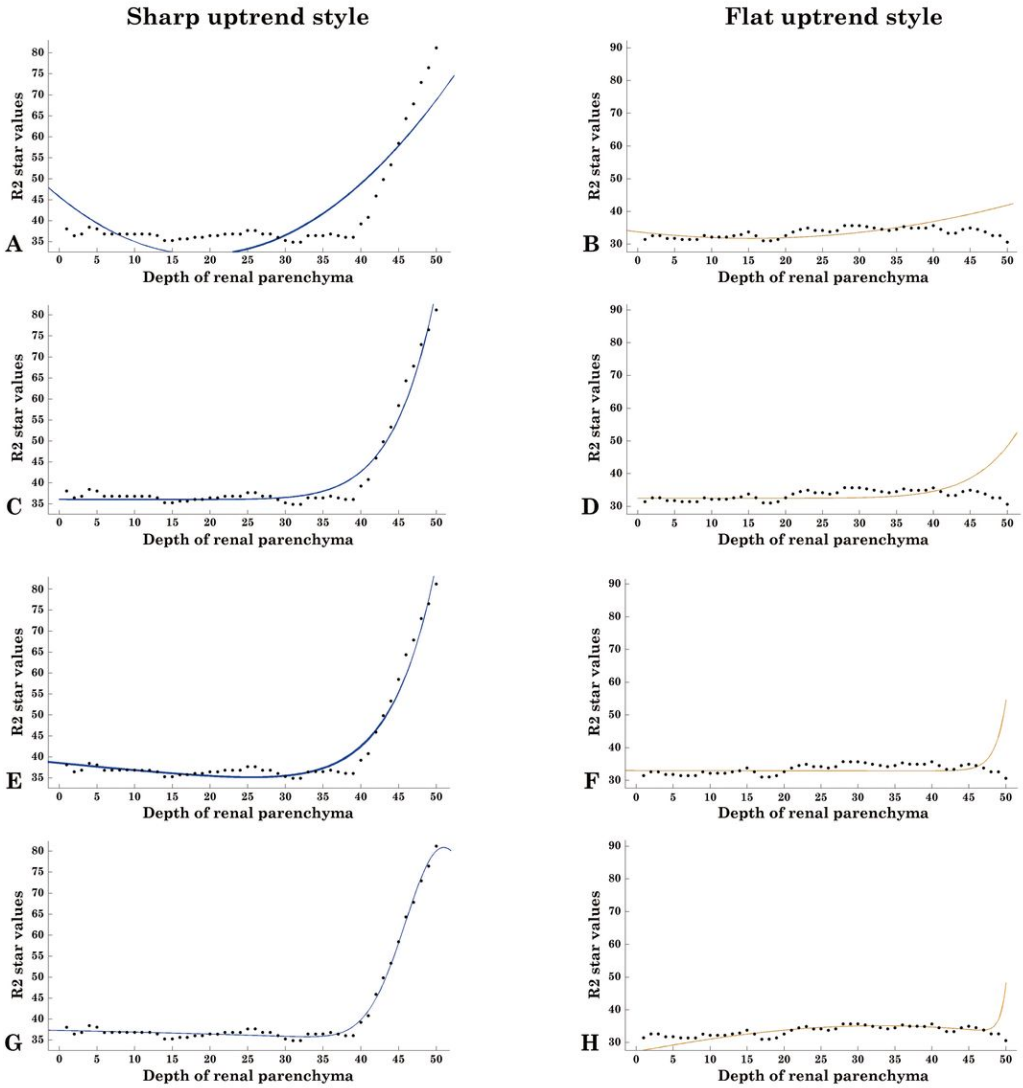

Figure 4

Comparison of the goodness of fit for four mathematic formulas in both the sharply raising style and the slowly raising style of R2* data in one patient with LN. Black dots indicate R2* values from the superficial cortical zone to the deep medullary zone. Blue and orange fitted curves are displayed in both the sharply raising style and the slowly raising style of R2* data, respectively. Fitted curves from four mathematic functions—Polynomial formula (A and B), formula (C and D), exponential formula (E and F), and Gaussian formula (G and H)—are arranged from top to bottom.

Supplementary Files

This is a list of supplementary files associated with this preprint. Click to download.

- ExcelFile1.xlsx
- ExcelFile2.xlsx